Experimental realization of quantum walks near synthetic horizons on photonic lattices

Runqiu He [1,*] Yule Zhao,[1,*] Chong Sheng [1,2,*,†] Jiachen Duan,[1] Ying Wei [1] Changwei Sun,[1] Liangliang Lu,[1,3,‡]
Yan-Xiao Gong [1,§] Shining Zhu,[1] and Hui Liu[1,¶]

[1]*National Laboratory of Solid State Microstructures and School of Physics, Collaborative Innovation Center of Advanced Microstructures,*
Nanjing University, Nanjing, Jiangsu 210093, China
[2]*Key Laboratory of Quantum Materials and Devices (Southeast University), Ministry of Education, Nanjing 211189, China*
[3]*Key Laboratory of Optoelectronic Technology of Jiangsu Province, School of Physical Science and Technology,*
Nanjing Normal University, Nanjing 210023, China

Entanglement plays crucial roles in quantum optics, providing a prerequisite for these recent unprecedented leaps. Nevertheless, the study of quantum entanglement under the influence of relativity, an important ingredient of quantum optics, still needs to be explored. In parallel, integrated photonic chips, particularly those with the aid of transformation optics, have simulated various relativity phenomena including gravitational lensing and Unruh radiation. However, thus far, studying relativistic quantum optics on this type of platform has not yet occurred. Here, we propose and experimentally realize quantum walks of entangled photons near an emulated Rindler horizon. Remarkably, we find that quantum interference near the synthetic horizon leads to a counterintuitive phenomenon of optical escape. Our study paves the way to a tabletop platform for studying quantum phenomena in various relativistic space-time metrics, and may bring an implication for the test of quantum theory in relativity.

I. INTRODUCTION

Quantum walks (QWs), the quantum mechanics analog of classical random walks [1], are a powerful tool used in quantum computing and simulation. In contrast to classical random walks, QWs have the distinct advantages of coherent superposition and quantum interference, making them a compelling platform for simulating topological physical phenomena [2–4], constructing novel quantum algorithms [5–7], and realizing universal quantum computing [8,9]. The implementation of QWs has been achieved with diverse physical architectures, ranging from nuclear magnetic resonance [10], trapped atoms and ions [11,12], superconducting systems [4], and fibers [13] to bulk optics [2] and especially integrated photonic circuits [14–19]. Among these architectures, silicon photonics [20], which are compatible with complementary metal-oxide-semiconductor fabrication, have been assumed to be a promising platform for QWs due to their overwhelming dominance in terms of density and performance. As a result, QWs on silicon can be adopted as a resource structure for quantum simulations, such as the environment-assisted quantum transports [21] and vibronic modes of molecules in chemistry [22]. Recently, there has been an increasing interest in quantum simulation under the background of relativity [23–28]. For example, QWs in a superconducting processor [28] with tunable couplings have simulated a curved space-time of black holes and observed an analogy of Hawking radiation. In addition to the analog of Hawking radiation [29,30], one of the salient examples is the Unruh effect [31,32] in flat space-time, which has been well emulated using a variety of quantum architectures [33–36].

At the same time, recent years have witnessed remarkable progress in the highly efficient manipulation of electromagnetic waves on the subwavelength scale using metamaterials [37], as well as the production of various functional photonic architectures with unprecedented performance in integrated photonic chips, e.g., polarization beam splitters and rotators [38,39], waveguide crossings and bends [40], and mode converters and multiplexers [41,42]. In particular, the emerging concept of transformation optics [43–45], a design method for controlling photons at a researcher's discretion, opens up unique possibilities for advancing the integration of complex functionalities in photonic circuits, such as Maxwell's fisheye lens for multimode routing [46], a Mikaelian lens for transporting coding information [47], and other various lenses [48,49]. Additionally, optical simulations of large-scale astrophysical phenomena using small-scale photonic chips [50], e.g., gravitational lensing [51], cosmic strings [52], a wormhole [53], and Dirac particles near the event horizon [25], have also been successfully achieved with transformation optics. Nevertheless, in all these experiments, simulations were carried out using either a classical Gaussian or a single-photon wave packet, both of which could be explained classically. Based on this background, our previous work [54] theoretically proposed the use of the QWs of entangled photons

---

*These authors contributed equally to this work.

†csheng@nju.edu.cn

‡liangliangl u@nju.edu.cn

§gongyanxiao@nju.edu.cn

¶liuhui@nju.edu.cn

to study quantum interference in a noninertial frame with a Rindler metric that is emulated by a nonuniform photonic lattice with the aid of transformation optics. Thus far, however, no experiments have been carried out for quantum interference of entangled photons in the emulated Rindler space using transformation optics. Remarkably, studying relativistic quantum optics in the tabletop platform may provide a forward-looking insight for quantum field theory in relativity in the future.

In this work, we present an observation of the QWs of entangled photons near an emulated horizon. We exploit silicon-on-insulator (SOI) technology to fabricate a nonuniform silicon waveguide lattice with site-dependent coupling coefficients inspired by transformation optics, which can map the Rindler space with an event horizon. We find that the QWs of single photons and two indistinguishable photons exhibit optical trapping near the emulated horizons, which is a well-known classical physical process in which light is trapping around the event horizon. Intriguingly, for a certain type of path-entangled photon, there is a counterintuitive phenomenon of optical escape arising from quantum interference.

II. THEORY

A. The mapping of Rindler metric based on transformation optics

To study the QWs of entangled photons near the emulated horizon on a silicon chip, we first map the $(1+1)$-dimensional Rindler metric [55] into one-dimensional waveguide lattices whose metric is

$$ds^2 = -(\alpha x)^2 dt^2 + dx^2, \quad (1)$$

where α is the acceleration and nature units have been adopted. Inspired by transformation optics, we exploit the invariance between the emulated and actual space-time as a tool to encode Rindler space-time into a lattice of coupled waveguides. When considering the motion of light, it satisfies null geodesic $ds = 0$. Then we obtain the evolution trajectory as $x \propto e^{\pm \alpha t}$. In parallel, when considering the dynamics of photons in the photonic lattice, it can be derived from a Schrodinger-type paraxial wave equation by employing the tight-binding approximation $i\partial\varphi_n/\partial z = \beta_0\varphi_n - \kappa_n\varphi_{n-1} - \kappa_{n+1}\varphi_{n+1}$, where φ_n is the complex field amplitude of site

n, z is the propagation distance along the waveguides, β_0 is the on-site energy of each waveguide, and parameter κ_n represents the coupling strength between the adjacent sites. Taking coupling coefficients as $\kappa_n = \kappa_{n+1} = \kappa$ and substituting the complex field amplitude with the plane-wave solution $\varphi_n \propto \exp(i\beta_x nd - i\beta_z z)$, we obtain the dispersion connecting transverse (β_x) and longitudinal (β_z) wave vectors as $\beta_z = \beta_0 - 2\kappa\cos(\beta_x d)$ (d is waveguide spacing). After the photons evolve in such a waveguide over distance Δz, each transverse component gains a phase $\Phi = \beta_z(\beta_x)\Delta z$, and the corresponding transverse shift of a wave centered around β_x is $\Delta x = \partial\Phi/\partial\beta_x = \Delta z\ \partial\beta_z/\partial\beta_x = \Delta z\ 2\kappa d\sin(\beta_x d)$. Because the propagation distance z in the coupled waveguide equation plays the role of the time in the Schrodinger equation, we can define the velocity of wave packets in such a system as $v = \Delta x/\Delta z = \partial\beta_z/\partial\beta_x = 2\kappa d\sin(\beta_x d)$. According to transformation optics, we find that for a lattice of identical waveguides whose coupling coefficient satisfies as $\kappa = \alpha n\kappa_0/2$ (κ_0 is the normalized coupling coefficient), the evolution of a Gaussian wave packet with an arbitrary transverse wave vector can be depicted as $\langle n \rangle \propto e^{\alpha\sin(\beta_x d)z}$, also determined by the acceleration α in the Rindler metric (see Appendix A). And the $n = 0$ waveguide acts as the Rindler horizon, as shown in Fig. 1(a).

B. The Green's function of light near Rindler horizon

Moreover, we further quantize the fields in the lattice to study the propagation of the photons. Because each waveguide supports a single mode, the field in waveguide n is represented by the bosonic creation and annihilation operators $a_n^\dagger$ and a_n, which satisfies the commutation relationship $[\ a_m,\ a_n^\dagger\ ] = \delta_{m,n}$. The Heisenberg equations for waveguide lattices with site-dependent coupling coefficients using identical waveguides can be described as $-i\partial a_n^\dagger/\partial z = \alpha(n-1)\kappa_0 a_{n-1}^\dagger/2 + \alpha n\kappa_0 a_{n+1}^\dagger/2$, where z is the spatial coordinate along the propagation axis, taking the role of time for the waveguide evolution. The evolution of the creation and annihilation operators is calculated using the Green's function $U_{m,n}(z)$ of the above equation, $a_m^\dagger(z) = \sum_n U_{m,n}(z)a_n^\dagger(z = 0)$. The unitary transformation $U_{m,n}(z)$ describes the amplitude for the transition of a single photon from waveguide n to waveguide m. The Green's function is given by (see Appendix B)

$$U_{m,n}(z) = \frac{1}{2\pi}\int_{-\pi}^{\pi} dq \exp\left\{imq - i2n\arctan\left[\tanh\left(\text{arctanh}\left[\tan\frac{q}{2}\right] - \frac{\alpha k_0 z}{2}\right)\right]\right\}, \quad (2)$$

where the quasimomentum q is confined to the zone $-\pi \leqslant q \leqslant \pi$. Since any input state can be expressed with the creation operators $a_m^\dagger$ and the vacuum state $|0\rangle$, the QWs of the photons in the emulated noninertial frame with a Rindler metric can be calculated using this type of Green's function.

III. EXPERIMENT

A. Quantum walks of single photons

In experiments, we fabricate a nonuniform photonic lattice [Fig. 1(a)] by judiciously varying the distance between

two adjacent identical waveguides as sites according to the relationship of the coupling coefficient with the distance of each waveguide [Fig. 1(b)], satisfying the special relationship required by the Rindler metric [Fig. 1(e)]. To study the evolution of photons near the Rindler horizon emulated by this type of nonuniform silicon lattice, we choose several waveguides near the Rindler horizon sites as sources for injecting photons [Fig. 1(d)]. For the detection of photons after passage through such a silicon lattice, we then select the next-nearest neighbor waveguide as the output source [Fig. 1(f)]. The selection of one waveguide site separated by another site can efficiently
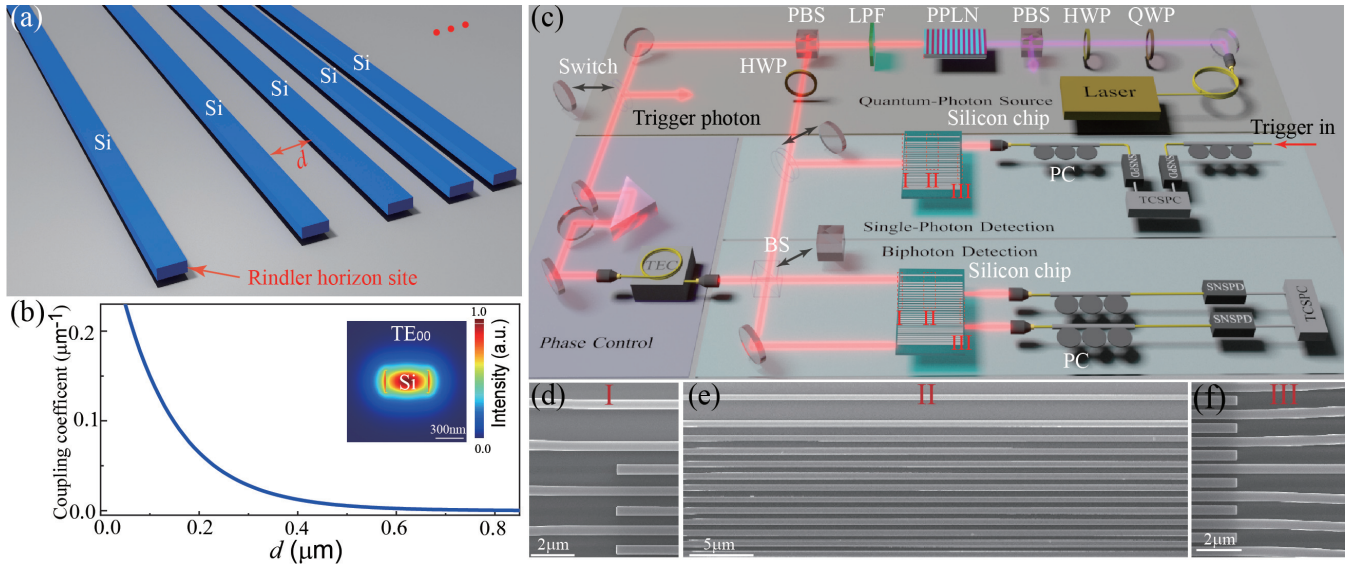
FIG. 1. Nonuniform silicon lattices and experiment setup. (a) Schematic of the nonuniform silicon lattice. (b) The coupling coefficient depending on the distance between the identical waveguides described as $\kappa \cong c_0 e^{-\eta d}$ ($c_0 = 0.3495\ \mu m^{-1}$, $\eta = 8.456\ \mu m^{-1}$). The fundamental mode (TE_{00}) is used. (c) Experimental setup consists of three parts, including the quantum light source, phase control, and photon detection. (d)–(f) A scanning electron microscope image of the input ports (zone I), evolution part (zone II), and output ports (zone III). The silicon lattice consists of 50 sites. In experiments, the insert loss on the silicon chips is about 7 dB.

avoid the extra unnecessary coupling between photons in the transporting region. Additionally, different types of quantum light sources are prepared with spontaneous parametric down-conversion by pumping a type II periodically poled lithium-niobate (PPLN) waveguide (see Appendix C). For all the data for coincidence detection in the experiments, accidental coincidence counts are subtracted.

First, we experimentally measure the QWs of single photons in the emulated Rindler horizon. For this case, we inject a heralded single photon into silicon chips for the evolution, while another photon acts as a trigger signal. Figure 2(a) theoretically exhibits the evolution probability of single photons located at site m when a photon is injected into the lattice at site $n_0 = 5$ using Green's functions, which are characterized by the photon density $\rho_m = \langle a_m^\dagger a_m \rangle = |U_{m,n_0}|^2$. The QWs of the single photons in the emulated noninertial frame exhibit an accelerated behavior. Single photons spread across the lattice by tunneling between waveguides in a pattern characterized by two peaks at the edges of the distribution. Both of the contours of the two peaks have an exponential form that is dependent on the acceleration α, in contrast to the two strong and linear ballistic lobes in the flat space. The left peak toward the Rindler horizon site is dominant, whereas the right peak away from the horizon becomes weak with the longer propagation distance. These phenomena can be explained from the perspective of the Green's function. When photons propagate over a large distance for $z \gg 2/(\alpha k_0)$, the Green's function can be simplified as $U_{m,n}(z) \cong \delta(m) \exp(in\pi/2)$, indicating that photons are always captured at the Rindler horizon site no matter which sites a photon is injected into. In experiments, we fabricate three nonuniform silicon lattices with different propagation lengths for the QWs of single photons with the same injecting site. The experimental and simulated results are illustrated in Figs. 2(b)–2(d). Moreover, the similarity between these patterns of the QWs of single photons is calculated as [19] $S = (\sum_j \sqrt{\rho_j^{expt} \rho_j^{theor}})^2 / (\sum_j \rho_j^{exp} \sum_j \rho_j^{theor})$,
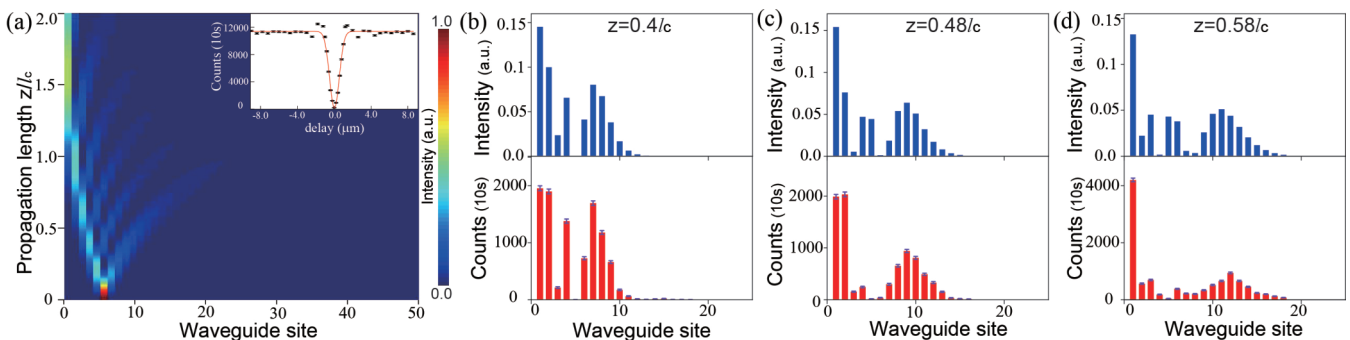

FIG. 2. Quantum walks of single photons. (a) Simulation of the evolution probability of single photons. The inset shows the HOM interference fringe with a visibility of $97.32\% \pm 0.17\%$. (b)–(d) The comparison of the detection probability of single photons between the measured and simulated results for different evolution distances ($l_c = 1000\ \mu m$). The uncertainties denote the standard deviations from the Poisson distribution of the raw photon counts.
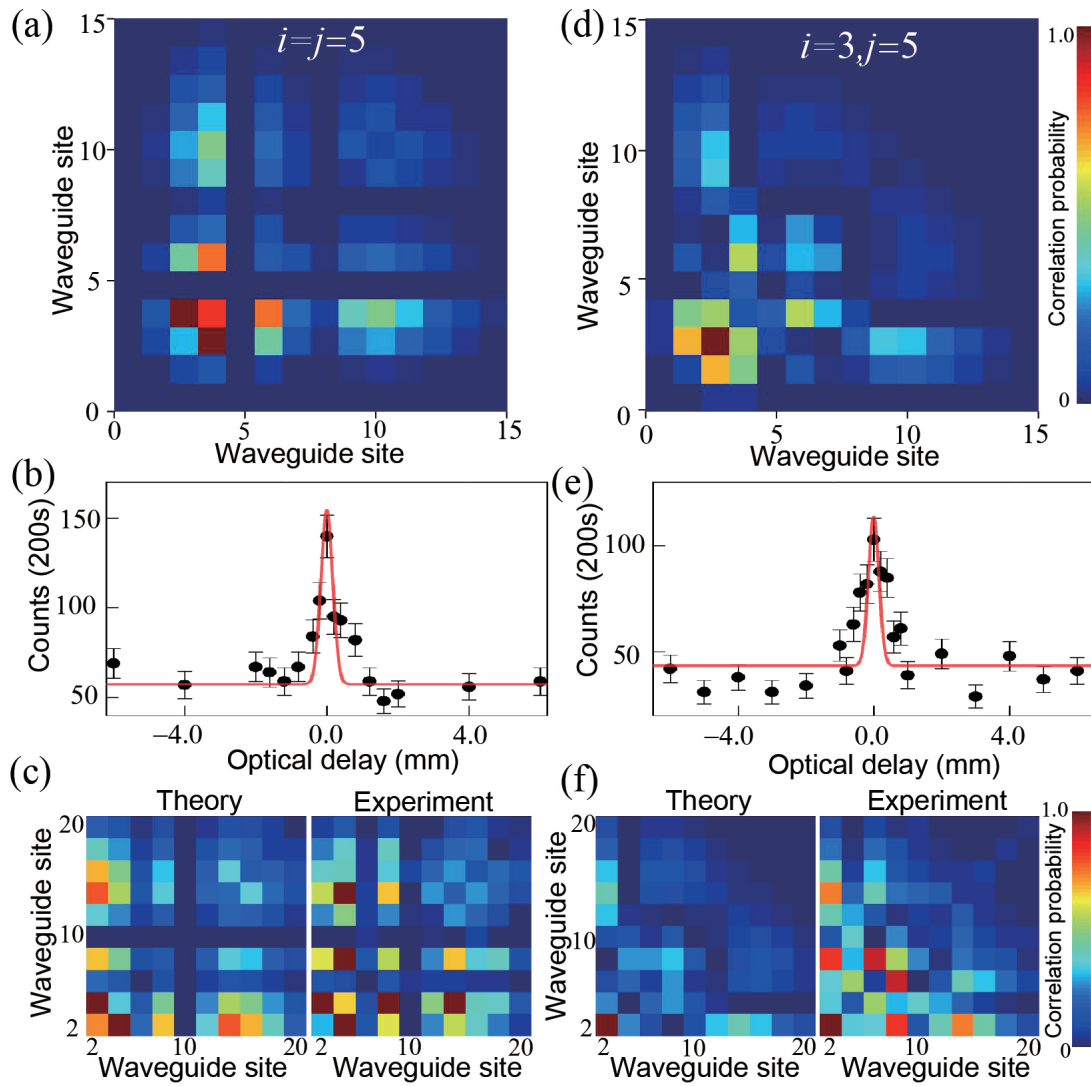
FIG. 3. Quantum walks of two indistinguishable photons. (a),(d) Simulated correlation probability when two photons are coupled into the same waveguide site and into different waveguide sites. (b),(e) Photon bunching curve retrieved from site 2 depending on the optical delay. (c),(f) The comparison of the correlation probability between the measured and simulated results for these two injecting methods. The evolution length is 400 μm. In experiment, we select the next-nearest neighbor waveguide as the output source. Correspondingly, these chosen sites in (a) shape the theory part of (c) made as a comparison for experimental results. The same principle is also applied to the comparison of (d)–(f) and Figs. 4(b), 4(c), 4(e), and 4(f).

with results of up to $85.15\% \pm 1.8\%$, $89.7\% \pm 1.5\%$, and $90.0\% \pm 0.3\%$. Both the experimental and the theoretical results validate the trapping process of single photons near the emulated Rindler horizon. Note that in experiments we inject single photons into photonic lattices through a single waveguide site and the QWs of single photons can be assumed as the superposition of null geodesics of a massless particle with various transverse vectors (see Appendix A). Whereas in Ref. [24], a broad Gaussian wave packet was utilized in the theoretical model of QWs, which chose a certain constant of the transverse vector and then clearly exhibited a null geodesic behavior of a massless particle.

B. Quantum walks of two indistinguishable photons

Furthermore, to study multiparticle interferences in the emulated accelerated noninertial frame, the two-photon

correlation function is introduced as $\Gamma_{i',j'}^{(i,j)} = \frac{1}{1+\delta_{i',j'}} |U_{i',i}(z)U_{j',j}(z) + U_{i',j}(z)U_{j',i}(z)|^2$, the probability of detecting one photon at waveguide i' and another photon at waveguide j', where i (i') and j (j') represent the input (output) sites. Figures 3(a) and 3(d) show the simulated correlation of indistinguishable photons when the two photons are injected into the same waveguide site $a_5^\dagger a_5^\dagger |0\rangle$ and coupled into different waveguide sites $a_3^\dagger a_5^\dagger |0\rangle$. In experiment, to realize two indistinguishable photons, we should choose one output port among the photonic lattice to measure coincident counts for the two injecting photons. If photons are indistinguishable, the photon bunching occurs and there is a peak value of coincident counts. Because the count rate in site 2 is highest among the output ports, we hence choose site 2 to measure coincident counts for the two injecting photons. Then we collect
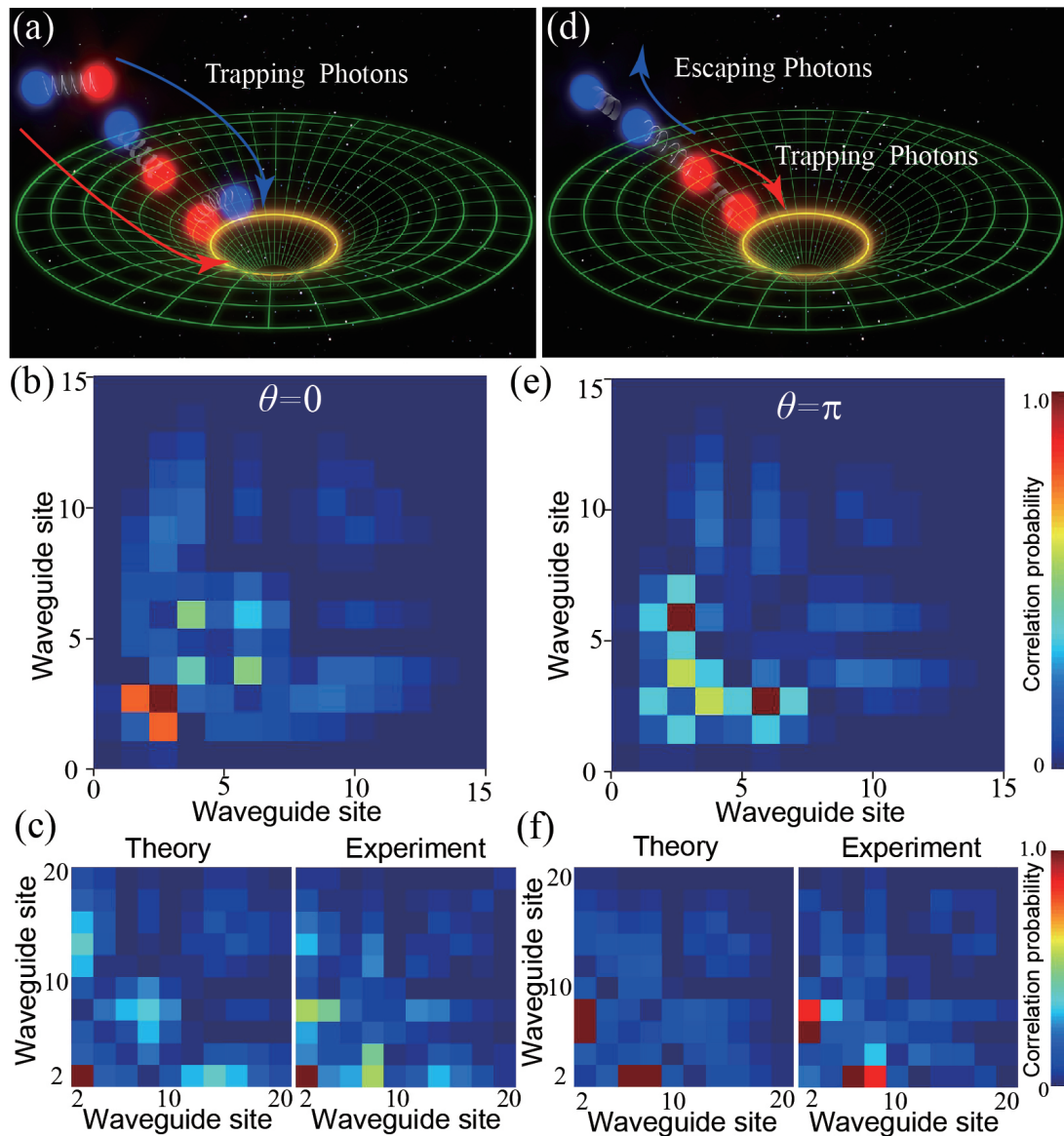
FIG. 4. Quantum walks of path-entangled photons. (a),(d) The schematic of the photon trapping and photon escape near the Rindler horizon. (b),(e) Simulated correlation probability for injecting path-entangled NOON photons with $\theta = 0$ and $\theta = \pi$. (c),(f) The comparison of the correlation probability between the measured and simulated results for these two different phases.

coincident counts for each data point from the balanced beam splitter by introducing phase delays using a high-precision computer-controlled translation stage. As shown in Figs. 3(b) and 3(e), a distinct quantum interference peak, whose value is nearly twice that of the distinguishable case, indicates that these two photons are highly indistinguishable [19]. Figure 3(c) compares the theoretical and experimental distribution of the coincident probability at a propagation length ($z = 400\,\mu\text{m}$) when two indistinguishable photons are coupled into the same site, while Fig. 3(f) illustrates the case for two photons injected into different sites at the same propagation length. We calculate the similarity between the two matrices of the simulated and measured results defined by [19] $S^{(1,1)} = (\sum_{i,j} \sqrt{\Gamma_{i,j}^{\text{expt}} \Gamma_{i,j}^{\text{theor}}})^2 / (\sum_{i,j} \Gamma_{i,j}^{\text{expt}} \sum_j \Gamma_{i,j}^{\text{theor}})$ to characterize the discrepancy between the experiment and theory. For these two different injecting cases, the experiment results reveal similarities of $93.0\% \pm 0.22\%$

and $85.15\% \pm 0.12\%$ relative to the simulations. The deviation comes from the imperfection of the photon indistinguishability and especially the divergence of coupling efficiency using grating coupling. Notably, two indistinguishable photons coupled into different waveguide sites have a larger deviation compared with the case of the same waveguide site. Additionally, considering the fabrication level of SOI technology and the brightness of the quantum light source at the current, the QWs of two photons with the long enough propagation length in a photonic lattice have not been achieved. Nevertheless, under the case of the limited propagation length ($z = 400\,\mu\text{m}$), we still find the bunching behavior that two photons have a high probability of concentrating around site 2. Despite not concentrating at site 0, all these theoretical and experimental results clearly reveal that two photons have a trend of bunching toward the Rindler horizon.

C. Quantum walks of path-entangled NOON states

In addition to indistinguishable photons, what happens to the entangled photons in the emulated accelerated noninertial frame involves more attraction. The entanglement is a counteractive feature of quantum physics that is at the heart of quantum technology. In experiments, we generate path-entangled NOON states [56,57] with $N = 2$ injected into two waveguides $|\psi\rangle = \frac{1}{2}(a_i^{\dagger 2} + e^{i\theta} a_j^{\dagger 2})|0\rangle$ ($i = 3, j = 5$) with a different phase θ. Note that NOON states, as a special type of nonclassical optical states, have important quantum technology applications, such as quantum computing [58], quantum optical metrology [59], as well as quantum lithography [60]; while to depict the evolution of path-entangled NOON states among the designed photonic lattices, we also employ a photon correlation function $\Gamma_{i',j'}^{(i,j)} = \frac{1}{1+\delta_{i',j'}}|U_{i',i}(z)U_{j',i}(z) + e^{i\theta}U_{i',j}(z)U_{j',j}(z)|^2$ to depict the nonclassical features of these NOON states [61,62]. Figure 4(b) depicts the simulation of the correlation distribution for the input NOON state with $\theta = 0$. And the photon correlation function for such a NOON state can be described as $\Gamma_{i',j'}^{(i,j)} = \frac{1}{1+\delta_{i',j'}}|U_{i',i}(z)U_{j',i}(z) + U_{i',j}(z)U_{j',j}(z)|^2$, indicating that the constructive interference occurs near the emulated Rindler horizon, which is alike the case of two indistinguishable photons having a high probability of bunching toward the horizon. And the experimental results agree with simulation results, as shown in Fig. 4(c), having a similarity of $85.38\% \pm 0.62\%$. Despite some deviation, both the simulation and the experimental results clearly exhibit the fact that the photons are bunching toward the Rindler horizon, which conforms to the expectation that photons are captured toward the synthetic horizon. Counterintuitively, for the input NOON state ($|\psi\rangle = \frac{1}{2}(a_i^{\dagger 2} - a_j^{\dagger 2})|0\rangle$) with $\theta = \pi$, we also obtain the photon correlation function described as $\Gamma_{i',j'}^{(i,j)} = \frac{1}{1+\delta_{i',j'}}|U_{i',i}(z)U_{j',i}(z) - U_{i',j}(z)U_{j',j}(z)|^2$. Obviously, the destructive interference of two such photons happens near the emulated Rindler horizon, whose behavior leads to photon escape and antibunching behavior. And we find that one photon is captured toward the Rindler horizon, whereas the other photon has a very high probability of escaping from the Rindler horizon, as shown in Figs. 4(d)–4(f). Additionally, the experimental results fit the theoretical result with a similarity of $88.38\% \pm 0.49\%$. Just as mentioned in Ref. [54], this photon escape is completely distinct from the Hawking mechanism that is caused by vacuum fluctuation generating particle pairs with positive and negative energy. The particles with negative energy are captured by the horizon, whereas the particles with positive energy escape. In contrast, when such entangled photons are walking near the emulated horizons, the quantum interference leads to quantum antibunching behavior resulting in that one photon is captured toward the emulated horizon, whereas the other photon has a very high probability of escaping.

IV. DISCUSSION

In conclusion, we have experimentally realized the QWs of single photons, two indistinguishable photons, and entangled photons in a synthetic horizon using silicon photonics.

The QWs of single photons and two indistinguishable photons exhibit optical trapping, a well-known classical physical recognition of the light trapping around the horizon. Remarkably, due to the antibunching behavior caused by quantum interference, a counterintuitive phenomenon of optical escape is observed for a certain type of path-entangled photon. In this work we exploit silicon photonics to conduct QWs for simulating quantum effects in a noninertial frame predicted by our previous theoretical work [54]. These types of nonuniform silicon photonic lattices inspired by transformation optics may provide a promising platform to give an insight into the future development of relativistic quantum optics. In the current work, the quantum state of light propagating in the emulated Rindler space is generated externally rather than internally. Note that silicon itself owns third-order nonlinear coefficients and has been extensively made as an integrated quantum light source. The production and evolution of a quantum state in Rindler space emulated by a single silicon chip is expected to be explored.

APPENDIX A: THE MAPPING RELATION BETWEEN NONUNIFORM WAVEGUIDE LATTICES AND SPACE-TIME WITH RINDLER METRIC

We consider the line element of a two-dimensional Schwarzschild space-time with only radical direction ($d\theta = 0, d\varphi = 0$)

$$ds^2 = -(1 - r_s/r)dt^2 + (1 - r_s/r)^{-1}dr^2. \quad (A1)$$

Here r_s is the radius of the Schwarzschild black hole. When considering the space near the event horizon $r = r_s + \rho^2/4r_s$ and $0 < \rho \ll r_s$, the term of Schwarzschild metric has a simplified form, $1 - r_s/r = 1 - (1 + \rho^2/4r_s^2)^{-1} \cong \rho^2/4r_s^2$. Thus, Eq. (A1) can be written as $ds^2 = -(\rho/2r_s)^2 dt^2 + d\rho^2$, which has the same form as the Rindler metric. Moreover, the curvature $1/2r_s$ plays the role of the acceleration α in the Rindler metric.

Here we present the details of the derivation of the mapping relation between nonuniform waveguide lattices and space-time with the Rindler metric. When considering the motion of light, it satisfies null geodesic $ds = 0$. Then we obtain the evolution trajectory as $x \propto e^{\pm \alpha t}$. On the other hand, according to transformation optics, the evolution of photons in the Rindler metric as Eq. (A1) is equivalent to that propagated in such a medium:

$$n_{\text{eff}} = \sqrt{-g_{11}/g_{00}} = 1/\alpha x, \quad (A2)$$

where $g_{00} = -\alpha^2 x^2$, $g_{11} = 1$. And photons evolve in such a medium and have a corresponding velocity as

$$v = 1/n_{\text{eff}} = \alpha x. \tag{A3}$$

Here nature units have been adopted ($G = c = 1$).

We exploit evanescently coupled photonic waveguide lattices with designed coupling coefficients to achieve the required inhomogeneous effective refractive index. The dynamics of a single-photon wave packet in a photonic waveguide lattice can be described by a set of coupled discrete Schrodinger equations, which are derived from a Schrodinger-type paraxial wave equation by employing the tight-binding approximation:

$$i\partial\varphi_m/\partial z = \beta_0\varphi_m - \kappa_m\varphi_{m-1} - \kappa_{m+1}\varphi_{m+1}, \tag{A4}$$

where φ_m is the complex field amplitude of site m, z is the propagation distance along the waveguides mapping the time variable, β_0 is the on-site energy of each waveguide, and parameter κ_m represents the coupling strength between the adjacent sites. Taking coupling coefficients as $\kappa_m = \kappa_{m+1} = \kappa$ and substituting the complex field amplitude with the plane-wave solution $\varphi_m = A\exp(i\beta_x md - i\beta_z z)$ (A is the amplitude of the plane wave), we obtain the dispersion connecting transverse and longitudinal dynamics as

$$\beta_z = \beta_0 - 2\kappa\cos(\beta_x d), \tag{A5}$$

where β_x (β_z) is the transverse (longitudinal) wave vector and d is the waveguide spacing. After the photons evolve in such a waveguide over distance Δz, each transverse component gains a phase $\Phi = \beta_z(\beta_x)\Delta z$, and the corresponding transverse shift of a wave centered around β_x is $\Delta x = \partial\Phi/\partial\beta_x = \Delta z\,\partial\beta_z/\partial\beta_x$. Because the propagation distance z in the coupled waveguide equation plays the role of the time t in the Schrodinger equation, we define the velocity of wave packets in such a system as

$$v = \Delta x/\Delta z = \partial\beta_z/\partial\beta_x = 2\kappa d\sin(\beta_x d). \tag{A6}$$

Note that when photons walk among such a photonic lattice, they have various velocity components caused by different transverse wave vector β_x. To map the propagation trajectory of photons under the Rindler metric into the discrete photonic lattice, by comparing Eqs. (A3) and (A6) and the discretization processing, we obtain the coupling coefficients as

$$\kappa/\kappa_0 = \alpha m/2. \tag{A7}$$

Here we take $x = md$, where m is waveguide sites and κ_0 is the normalized coupling coefficient.

As a comparison, we first numerically calculate the light propagation of classical Gaussian wave packets with various transverse wave vectors in the uniform lattice. Figures 5(a1)–5(c2) clearly exhibit the evolution of the wave packet with a constant transverse wave vector, whose value determines the evolution velocity. And the movement of the center of classical Gaussian wave packets $\langle n \rangle$ is linearly proportional to the propagation length [see Figs. 5(d1) and 5(d2)]. Therefore, the uniform photonic lattice can well replicate the null geodesic behavior of photons with the different velocity in the flat space. And the Gaussian wave packet with the transverse wave

vector $\beta_x = \pm\pi/(2d)$ has the highest value of velocity. Likewise, Figs. 5(e1)–5(g2) also exhibit the evolution of the wave packet with various transverse wave vectors in the emulated Rindler space. In Figs. 5(h1) and 5(h2), we can see that the evolution of the center of a wave packet exponentially depends on the propagation length (note that the scale of the vertical axis is logarithmic), which can be depicted as $\langle n \rangle \propto e^{\alpha\sin(\beta_x d)z}$. Note that the Gaussian wave packet with the transverse wave vector $\beta_x = \pm\pi/(2d)$ has the fastest evolution, deciding the contour of the quantum walk.

APPENDIX B: THE GREEN'S FUNCTION OF THE ACCELERATED LATTICE

To obtain the Green's function of the emulated accelerated lattice with linear coupling coefficients as waveguide sites, we take the Hamilton operator

$$H = -\frac{\alpha\kappa_0}{2}\sum_{n=-\infty}^{n=+\infty} n(|n\rangle\langle n+1| + |n+1\rangle\langle n|)$$

$$+ \beta_0\sum_{n=-\infty}^{n=+\infty}|n\rangle\langle n|. \tag{B1}$$

Alternatively, one can use a representation in Bloch waves:

$$|k\rangle = \sum_{n=-\infty}^{n=+\infty}|n\rangle\langle n|k\rangle = \sqrt{\frac{1}{2\pi}}\sum_{n=-\infty}^{n=+\infty}|n\rangle e^{ink}, \tag{B2}$$

which satisfies the Bloch condition

$$\langle n+1|k\rangle = e^{ik}\langle n|k\rangle$$

with quasimomentum k confined to the Brillouin zone $-\pi \leqslant k \leqslant \pi$. By means of the identities

$$\sum_{n=-\infty}^{n=+\infty} n\langle k'|n+1\rangle\langle n|k\rangle = e^{-ik'}\sum_{n=-\infty}^{n=+\infty} n\langle k'|n\rangle\langle n|k\rangle$$

$$= e^{-ik'}\frac{1}{2\pi}\sum_{n=-\infty}^{n=+\infty} ne^{in(k-k')}$$

$$= -e^{-ik'}i\frac{\partial\delta(k'-k)}{\partial k}, \tag{B3}$$

$$\sum_{n=-\infty}^{n=+\infty} n\langle k'|n\rangle\langle n+1|k\rangle = e^{ik}\sum_{n=-\infty}^{n=+\infty} n\langle k'|n\rangle\langle n|k\rangle$$

$$= e^{ik}\frac{1}{2\pi}\sum_{n=-\infty}^{n=+\infty} ne^{in(k-k')}$$

$$= -e^{ik}i\frac{\partial\delta(k'-k)}{\partial k}. \tag{B4}$$

We obtain that the tight-binding Hamiltonian is diagonal:

$$\langle k'|H|k\rangle = \delta(k'-k)H(k), \tag{B5}$$

$$H(k) = -\alpha\kappa_0\cos(k)i\frac{\partial}{\partial k} + \beta_0. \tag{B6}$$

The eigenstates of the Hamiltonian are found by integrating the first-order differential equation,

$$-\alpha\kappa_0\cos(k)i\frac{\partial}{\partial k}\Psi(k) + \beta_0\Psi(k) = E\Psi(k) \tag{B7}$$
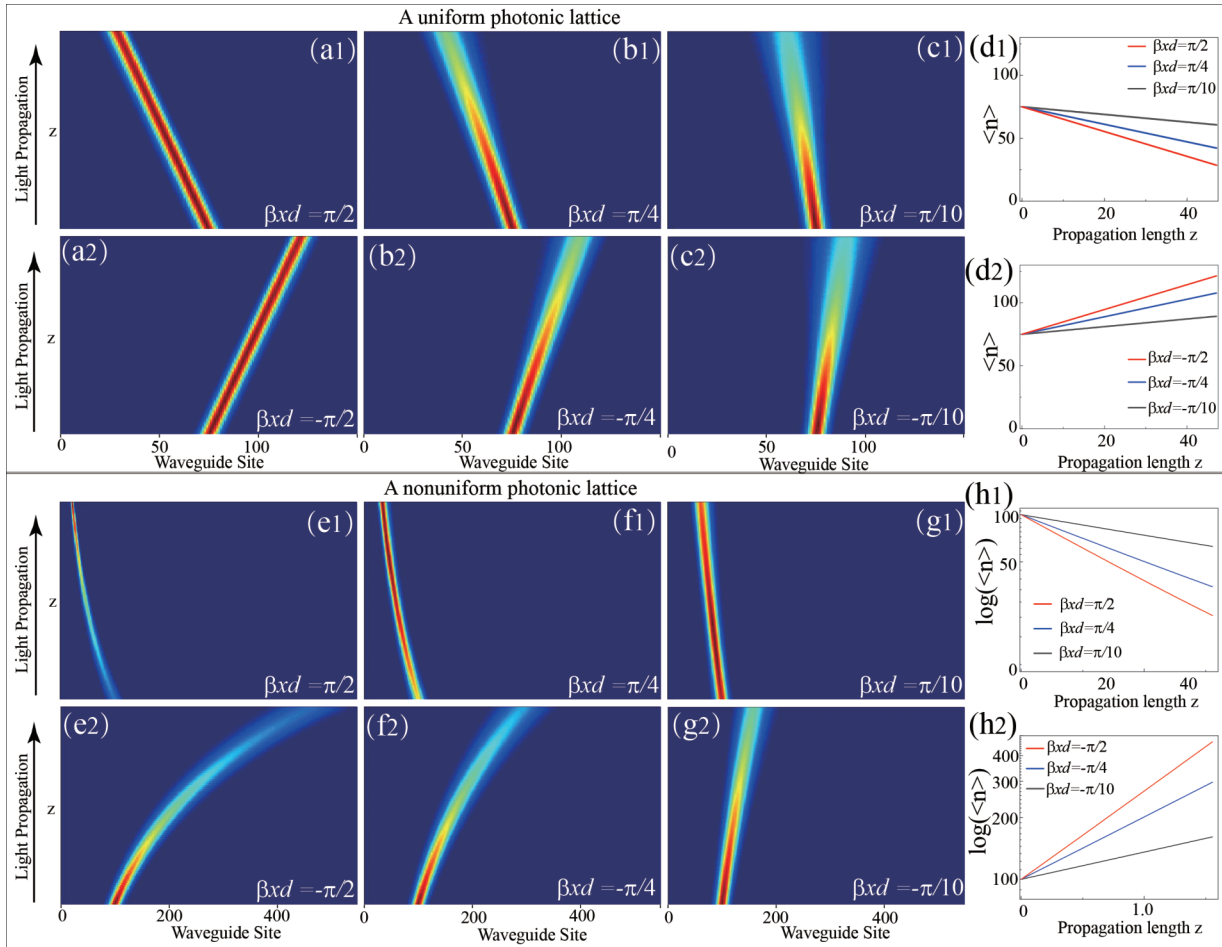
FIG. 5. A designed photonic lattice respectively emulates the null geodesic of photons in flat space (a1)–(c2) and Rindler space (e1)–(g2) when injecting a classic Gaussian wave packet with different transverse wave vectors. Figs. d1, d2, h1, and h2 are the evolution of the center of the wave packet.

with the periodic boundary condition $\Psi(k + 2\pi) = \Psi(k)$, and $E_m = \beta_0 - \frac{m\alpha\kappa_0}{2}$. One can rewrite Eq. (B7) as

$$\Psi_m(k) = \langle k | \Psi_m \rangle = \sqrt{\frac{1}{2\pi}} \exp\left[\frac{2(E_m - \beta_0) \text{arc} \tan \text{h}\left(\tan \frac{k}{2}\right)}{\alpha\kappa_0} \right] = \sqrt{\frac{1}{2\pi}} \exp\left[-im \,\text{arc} \tan \text{h}\left(\tan \frac{k}{2}\right) \right]. \tag{B8}$$

The description in terms of the Wannier states with the Fourier transformation is as follows:

$$\Psi_m(n) = \langle n | \Psi_m \rangle = \int_{-\pi}^{\pi} dk \langle n | k \rangle \langle k | \Psi_m \rangle = \frac{1}{2\pi} \int_{-\pi}^{\pi} dk \, e^{i\{nk - m \cdot \text{arc} \tan \text{h}[\tan (k/2)]\}}. \tag{B9}$$

In the basis of Wannier states one can obtain the propagator as

$$U_{nn'} = \langle n | U(z) | n' \rangle = \sum_l \langle n | \Psi_l \rangle e^{-iE_l z} \langle \Psi_l | n' \rangle$$

$$= \sum_l \frac{1}{2\pi} \int_{-\pi}^{\pi} dk \, e^{i\{nk - l \,\text{arc} \tan \text{h}[\tan (k/2)]\}} e^{-i[\beta_0 - (l\alpha\kappa_0/2)]z} \frac{1}{2\pi} \int_{-\pi}^{\pi} dk' e^{i\{-n'k' + l \,\text{arc} \tan \text{h}[\tan (k/2)]\}}$$

$$= \sum_l \frac{1}{2\pi} \frac{1}{2\pi} \int_{-\pi}^{\pi} \int_{-\pi}^{\pi} dk \, dk' e^{i\{nk - l \,\text{arc} \tan \text{h}[\tan(k/2)] - [\beta_0 - (l\alpha\kappa_0/2)]z - n'k' + l \,\text{arc} \tan \text{h}(\tan \frac{k'}{2})\}}$$

$$= \sum_l \frac{1}{2\pi} \frac{1}{2\pi} \int_{-\pi}^{\pi} \int_{-\pi}^{\pi} dk \, dk' e^{i\{nk - n'k' - \beta_0 z - l \,\text{arc} \tan \text{h}[\tan (k/2)] + l(\alpha\kappa_0 z/2) + l \,\text{arc} \tan \text{h}[\tan (k/2)]\}}$$

$$= \frac{1}{2\pi} \int_{-\pi}^{\pi} \int_{-\pi}^{\pi} dk\,dk'\, e^{i(nk - n'k' - \beta_0 z)} \delta\left[\operatorname{arc\,tan\,h}\left(\tan \frac{k}{2} \right) - \operatorname{arc\,tan\,h}\left(\tan \frac{k'}{2} \right) - \frac{\alpha \kappa_0 z}{2} \right]$$

$$= \frac{1}{2\pi} \int_{-\pi}^{\pi} dk \cdot \exp\left(ink - i2n' \operatorname{arc\,tan}\left\{ \tan h\left[\operatorname{arc\,tan\,h}\left(\tan \frac{k}{2} \right) - \frac{\alpha \kappa_0 z}{2} \right] \right\} - i\beta_0 z \right) \tag{B10}$$

when $\alpha \kappa_0 z / 2 \gg 1$, which means photons propagating with large enough distance, one can simplify the Green's function as

$$U_{nn'} \approx \frac{1}{2\pi} \int_{-\pi}^{\pi} dk \, \exp(ink) \exp\left(in' \frac{\pi}{2} - i\beta_0 z \right) = \delta(n) \exp\left(in' \frac{\pi}{2} - i\beta_0 z \right). \tag{B11}$$

APPENDIX C: EXPERIMENTAL METHODS

1. Sample fabrication

In the experiments, a structured nonuniform photonic lattice is fabricated by etching the device layer of an SOI wafer, with confinement provided by the buried oxide underneath and a capping oxide above. The thickness of the silicon device layer is 220 nm, while the buried oxide underneath and the capping oxide above are both 2-μm-thick silica. The waveguides are designed to be single mode, having a width of 450 nm. The structures are defined by electron beam lithography and dry etching. The coupling coefficient of the fundamental transverse electric mode at the telecom wavelength between two adjacent identical waveguides is dependent on the distance between them, which can be described as $\kappa \cong c_0 e^{-\eta d}$ with $c_0 = 0.3495 \ \mu m^{-1}$ and $\eta = 8.456 \ \mu m^{-1}$.

2. Quantum light source

We generate the single-photon pair at the wavelength of 1550.92 nm via spontaneous parametric down-conversion by pumping a type II PPLN waveguide from a continuous wave

fixed at 785.46 nm. And the length of the PPLN waveguide is 2 cm. The generated photon pair is separated into two components, horizontal and vertical polarization, after passing through a long-pass filter and a polarized beam splitter. Moreover, after converting the polarization of these types of single photons from the vertical state to the horizontal state, we find that the deterministically separated identical photon pair has a very high visibility of the quantum interferences, characterized by a Hong-Ou-Mandel (HOM) dip with $97.32\% \pm 0.17\%$ visibility.

3. Photon detection

Photons are filtered to suppress residual noise with off-chip filters and finally directed into and detected by superconducting nanowire single-photon detectors (SNSPDs). Fiber polarization controllers are used to optimize the polarization of the photons for the maximum detection efficiency in the SNSPDs. Coincidence measurements are performed using the time-correlated single-photon counting module (Picoquant PicoHarp 300).

[1] Y. Aharonov, L. Davidovich, and N. Zagury, Quantum random walks, Phys. Rev. A **48**, 1687 (1993).

[2] L. Xiao *et al.*, Observation of topological edge states in parity-time-symmetric quantum walks, Nat. Phys. **13**, 1117 (2017).

[3] Y. Wang, Y.-H. Lu, F. Mei, J. Gao, Z.-M. Li, H. Tang, S.-L. Zhu, S. Jia, and X.-M. Jin, Direct observation of topology from single-photon dynamics, Phys. Rev. Lett. **122**, 193903 (2019).

[4] M. Gong *et al.*, Quantum walks on a programmable two-dimensional 62-qubit superconducting processor, Science **372**, 948 (2021).

[5] N. Shenvi, J. Kempe, and K. B. Whaley, Quantum random-walk search algorithm, Phys. Rev. A **67**, 052307 (2003).

[6] J. B. Spring *et al.*, Boson sampling on a photonic chip, Science **339**, 798 (2013).

[7] H. Tang *et al.*, Experimental quantum fast hitting on hexagonal graphs, Nat. Photon. **12**, 754 (2018).

[8] A. M. Childs, Universal computation by quantum walk, Phys. Rev. Lett. **102**, 180501 (2009).

[9] A. M. Childs, D. Gosset, and Z. Webb, Universal computation by multiparticle quantum walk, Science **339**, 791 (2013).

[10] J. F. Du, H. Li, X. D. Xu, M. J. Shi, J. H. Wu, X. Y. Zhou, and R. D. Han, Experimental implementation of the quantum random-walk algorithm, Phys. Rev. A **67**, 042316 (2003).

[11] M. Karski, L. Foerster, J.-M. Choi, A. Steffen, W. Alt, D. Meschede, and A. Widera, Quantum walk in position space with single optically trapped atoms, Science **325**, 174 (2009).

[12] H. Schmitz, R. Matjeschk, C. Schneider, J. Glueckert, M. Enderlein, T. Huber, and T. Schaetz, Quantum walk of a trapped ion in phase space, Phys. Rev. Lett. **103**, 090504 (2009).

[13] H. Defienne, M. Barbieri, I. A. Walmsley, B. J. Smith, and S. Gigan, Two-photon quantum walk in a multimode fiber, Sci. Adv. **2**, e1501054 (2016).

[14] H. B. Perets, Y. Lahini, F. Pozzi, M. Sorel, R. Morandotti, and Y. Silberberg, Realization of quantum walks with negligible decoherence in waveguide lattices, Phys. Rev. Lett. **100**, 170506 (2008).

[15] A. Peruzzo *et al.*, Quantum walks of correlated photons, Science **329**, 1500 (2010).

[16] A. S. Solntsev, F. Setzpfandt, A. S. Clark, C. W. Wu, M. J. Collins, C. Xiong, A. Schreiber, F. Katzschmann, F. Eilenberger, R. Schiek, W. Sohler, A. Mitchell, C. Silberhorn, B. J. Eggleton, T. Pertsch, A. A. Sukhorukov, D. N. Neshev, and Y. S. Kivshar, Generation of nonclassical biphoton states through cascaded quantum walks on a nonlinear chip, Phys. Rev. X **4**, 031007 (2014).

[17] M. Lebugle, M. Graefe, R. Heilmann, A. Perez-Leija, S. Nolte, and A. Szameit, Experimental observation of NOON state Bloch oscillations, Nat. Commun. **6**, 8273 (2015).

[18] H. Tang *et al.*, Experimental two-dimensional quantum walk on a photonic chip, Sci. Adv. **4**, eaat3174 (2018).

[19] Z.-Q. Jiao, J. Gao, W.-H. Zhou, X.-W. Wang, R.-J. Ren, X.-Y. Xu, L.-F. Qiao, Y. Wang, and X.-M. Jin, Two-dimensional quantum walks of correlated photons, Optica **8**, 1129 (2021).

[20] J. W. Silverstone, D. Bonneau, J. L. O'Brien, and M. G. Thompson, Silicon quantum photonics, IEEE J. Sel. Top. Quantum Electron. **22**, 390 (2016).

[21] N. C. Harris *et al.*, Quantum transport simulations in a programmable nanophotonic processor, Nat. Photon. **11**, 447 (2017).

[22] C. Sparrow *et al.*, Simulating the vibrational quantum dynamics of molecules using photonics, Nature (London) **557**, 660 (2018).

[23] G. Di Molfetta, M. Brachet, and F. Debbasch, Quantum walks as massless Dirac fermions in curved space-time, Phys. Rev. A **88**, 042301 (2013).

[24] P. Arrighi, S. Facchini, and M. Forets, Quantum walking in curved spacetime, Quantum Inf. Process **15**, 3467 (2016).

[25] Y. Wang *et al.*, Quantum simulation of particle pair creation near the event horizon, Natl. Sci. Rev. **7**, 1476 (2020).

[26] I. Boettcher, P. Bienias, R. Belyansky, A. J. Kollar, and A. V. Gorshkov, Quantum simulation of hyperbolic space with circuit quantum electrodynamics: From graphs to geometry, Phys. Rev. A **102**, 032208 (2020).

[27] C. Morice, A. G. Moghaddam, D. Chernyavsky, J. van Wezel, and J. van den Brink, Synthetic gravitational horizons in low-dimensional quantum matter, Phys. Rev. Res. **3**, L022022 (2021).

[28] Y.-H. Shi *et al.*, Quantum simulation of Hawking radiation and curved spacetime with a superconducting on-chip black hole, Nat. Commun. **14**, 3263 (2023).

[29] J. R. M. de Nova, K. Golubkov, V. I. Kolobov, and J. Steinhauer, Observation of thermal Hawking radiation and its temperature in an analogue black hole, Nature (London) **569**, 688 (2019).

[30] J. Drori, Y. Rosenberg, D. Bermudez, Y. Silberberg, and U. Leonhardt, Observation of stimulated Hawking radiation in an optical analogue, Phys. Rev. Lett. **122**, 010404 (2019).

[31] W. G. Unruh, Experimental black-hole evaporation? Phys. Rev. Lett. **46**, 1351 (1981).

[32] L. C. B. Crispino, A. Higuchi, and G. E. A. Matsas, The Unruh effect and its applications, Rev. Mod. Phys. **80**, 787 (2008).

[33] I. I. Smolyaninov, Giant Unruh effect in hyperbolic metamaterial waveguides, Opt. Lett. **44**, 2224 (2019).

[34] J. Hu, L. Feng, Z. Zhang, and C. Chin, Quantum simulation of Unruh radiation, Nat. Phys. **15**, 785 (2019).

[35] H. Wang, M. P. Blencowe, C. M. Wilson, and A. J. Rimberg, Mechanically generating entangled photons from the vacuum: A microwave circuit-acoustic resonator analog of the oscillatory Unruh effect, Phys. Rev. A **99**, 053833 (2019).

[36] S. Onoe, T. L. M. Guedes, A. S. Moskalenko, A. Leitenstorfer, G. Burkard, and T. C. Ralph, Realizing a rapidly switched Unruh-DeWitt detector through electro-optic sampling of the electromagnetic vacuum, Phys. Rev. D **105**, 056023 (2022).

[37] J. B. Pendry, A. J. Holden, D. J. Robbins, and W. J. Stewart, Magnetism from conductors and enhanced nonlinear phenomena, IEEE Trans. Microwave Theory Tech. **47**, 2075 (1999).

[38] H. Xu, D. Dai, and Y. Shi, Ultra-broadband and ultra-compact on-chip silicon polarization beam splitter by using hetero-anisotropic metamaterials, Laser Photonics Rev. **13**, 1800349 (2019).

[39] H. Xu and Y. Shi, Subwavelength-grating-assisted silicon polarization rotator covering all optical communication bands, Opt. Express **27**, 5588 (2019).

[40] L. H. Gabrielli, D. Liu, S. G. Johnson, and M. Lipson, On-chip transformation optics for multimode waveguide bends, Nat. Commun. **3**, 1217 (2012).

[41] Z. Li *et al.*, Controlling propagation and coupling of waveguide modes using phase-gradient metasurfaces, Nat. Nanotechnol. **12**, 675 (2017).

[42] Y. Liu *et al.*, Arbitrarily routed mode-division multiplexed photonic circuits for dense integration, Nat. Commun. **10**, 3263 (2019).

[43] J. B. Pendry, D. Schurig, and D. R. Smith, Controlling electromagnetic fields, Science **312**, 1780 (2006).

[44] U. Leonhardt, Optical conformal mapping, Science **312**, 1777 (2006).

[45] H. Chen, C. T. Chan, and P. Sheng, Transformation optics and metamaterials, Nat. Mater. **9**, 387 (2010).

[46] S. Li, Y. Zhou, J. Dong, X. Zhang, E. Cassan, J. Hou, C. Yang, S. Chen, D. Gao, and H. Chen, Universal multimode waveguide crossing based on transformation optics, Optica **5**, 1549 (2018).

[47] X. Wang, H. Chen, H. Liu, L. Xu, C. Sheng, and S. Zhu, Self-focusing and the Talbot effect in conformal transformation optics, Phys. Rev. Lett. **119**, 033902 (2017).

[48] T. Zentgraf, Y. Liu, M. H. Mikkelsen, J. Valentine, and X. Zhang, Plasmonic Luneburg and Eaton lenses, Nat. Nanotechnol. **6**, 151 (2011).

[49] W. Qi, Y. Yu, and X. Zhang, On-chip arbitrary-mode spot size conversion, Nanophotonics **9**, 4365 (2020).

[50] R. Bekenstein, Y. Kabessa, Y. Sharabi, O. Tal, N. Engheta, G. Eisenstein, A. J. Agranat, and M. Segev, Control of light by curved space in nanophotonic structures, Nat. Photon. **11**, 664 (2017).

[51] C. Sheng, H. Liu, Y. Wang, S. N. Zhu, and D. A. Genov, Trapping light by mimicking gravitational lensing, Nat. Photon. **7**, 902 (2013).

[52] C. Sheng, H. Liu, H. Chen, and S. Zhu, Definite photon deflections of topological defects in metasurfaces and symmetry-breaking phase transitions with material loss, Nat. Commun. **9**, 4271 (2018).

[53] G. H. L. R. Q. He, S. N. Zhu, and H. Liu, Simulation of giant tidal force of wormhole using curved optical spaces, Phys. Rev. Res. **2**, 013237 (2020).

[54] C. Sheng, C. Huang, R. Yang, Y. Gong, S. Zhu, and H. Liu, Simulating the escape of entangled photons from the event horizon of black holes in nonuniform optical lattices, Phys. Rev. A **103**, 033703 (2021).

[55] R. M. Wald, *General Relativity* (University of Chicago Press, Chicago, 1981).

[56] P. Kok, H. Lee, and J. P. Dowling, Creation of large-photon-number path entanglement conditioned on photodetection, Phys. Rev. A **65**, 052104 (2002).

[57] G. J. Pryde and A. G. White, Creation of maximally entangled photon-number states using optical fiber multiports, Phys. Rev. A **68**, 052315 (2003).

[58] P. Kok, W. J. Munro, K. Nemoto, T. C. Ralph, J. P. Dowling, and G. J. Milburn, Linear optical quantum computing with photonic qubits, Rev. Mod. Phys. **79**, 135 (2007).

[59] J. P. Dowling, Quantum optical metrology – the lowdown on high-NOON states, Contemp. Phys. **49**, 125 (2008).

[60] A. N. Boto, P. Kok, D. S. Abrams, S. L. Braunstein, C. P. Williams, and J. P. Dowling, Quantum interferometric optical lithography: Exploiting entanglement to beat the diffraction limit, Phys. Rev. Lett. **85**, 2733 (2000).

[61] H. Jin, F. M. Liu, P. Xu, J. L. Xia, M. L. Zhong, Y. Yuan, J. W. Zhou, Y. X. Gong, W. Wang, and S. N. Zhu, On-chip generation and manipulation of entangled photons based on reconfigurable lithium-niobate waveguide circuits, Phys. Rev. Lett. **113**, 103601 (2014).

[62] J. W. Silverstone *et al.*, On-chip quantum interference between silicon photon-pair sources, Nat. Photon. **8**, 104 (2014).